Bioconjugate Chemistry

Article

pubs.acs.org/bc

# Cryptophane-Folate Biosensor for $^{129}$Xe NMR

Najat S. Khan, Brittany A. Riggle, Garry K. Seward, Yubin Bai, and Ivan J. Dmochowski*

Department of Chemistry, University of Pennsylvania, 231 South 34th Street, Philadelphia, Pennsylvania 19104, United States

Supporting Information

**ABSTRACT:** Folate-conjugated cryptophane was developed for targeting cryptophane to membrane-bound folate receptors that are overexpressed in many human cancers. The cryptophane biosensor was synthesized in 20 nonlinear steps, which included functionalization with folate recognition moiety, solubilizing peptide, and Cy3 fluorophore. Hyperpolarized $^{129}$Xe NMR studies confirmed xenon binding to the folate-conjugated cryptophane. Cellular internalization of biosensor was monitored by confocal laser scanning microscopy and quantified by flow cytometry. Competitive blocking studies confirmed cryptophane endocytosis through a folate receptor-mediated pathway. Flow cytometry revealed 10-fold higher cellular internalization in KB cancer cells overexpressing folate receptors compared to HT-1080 cells with normal folate receptor expression. The biosensor was determined to be nontoxic in HT-1080 and KB cells by MTT assay at low micromolar concentrations typically used for hyperpolarized $^{129}$Xe NMR experiments.

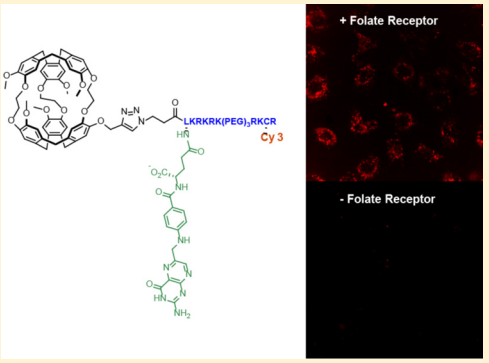


## INTRODUCTION

Magnetic resonance imaging (MRI) is a noninvasive medical imaging technique most useful for obtaining high contrast *in vivo* images of tissues, organs, and bone at high spatial resolution. $^{1}$H MRI is limited by low sensitivity, in part due to high background from endogenous proton signals. In order to increase signal, especially when imaging vascular tissues or analyzing brain perfusion, gadolinium- or iron-oxide-based contrast agents are commonly used. However, early and accurate diagnoses of human disease increasingly rely upon information gleaned from molecular imaging of protein biomarkers or metabolic processes. There are now many examples using PET and SPECT imaging agents with readily detected radioactive nuclei.[1] By comparison, current MRI contrast agents have limited ability to detect proteins or metabolites of low abundance in cells.[2−4] The goal of making "smart" MRI contrast agents that produce readily measured signals in response to environmental cues has led to intense investigation of nuclei that can be hyperpolarized (HP) to achieve a majority of unpaired nuclear spins, most commonly $^{13}$C, $^{3}$He, $^{129}$Xe, and $^{38}$Kr.[5−8] Recent applications of HP $^{13}$C pyruvate in human and small animal MRI highlight the great potential of hyperpolarization techniques for evaluating metabolites associated with prostate cancer and cardiac dysfunction.[9−11]

$^{129}$Xe is a nontoxic gas with high water solubility (4.2 mM atm$^{-1}$ at 300 K),[12] and unique physical−chemical properties that motivate the development of a new class of versatile MRI contrast agents. Xenon's significant polarizability contributes to its affinity for void spaces in natural[13] and synthetic materials,[14−17] as well as chemical-shift sensitivity to its molecular environment. Recent advances in $^{129}$Xe hyperpolarization technology make this agent now much more accessible, in liter quantities at near-unity polarization levels.[18] Several HP $^{129}$Xe MRI studies imaging the lungs and brain have been published, for both rodents and humans.[19−24]

Our laboratory has developed water-soluble tris(triazole ethylamine) and tris-carboxylate derivatives of cryptophane-A that bind xenon with usefully large association constants, $K_A$ = 17 000−42 000 M$^{-1}$ in buffer at 293 K.[25,26] Additionally, one tris-carboxylate cryptophane was shown to bind Xe in human plasma with appreciable affinity, $K_A$ = 22 000 M$^{-1}$ at 310 K.[25] The chemical shift of $^{129}$Xe-bound cryptophane can be modulated stereoelectronically, e.g., by ruthenating the aromatic rings,[27] varying the size of the cavity[28] or appending water-solubilizing moieties.[25,26,29] We and others have synthesized cryptophane biosensors that are conjugated to various ligands via a hydroxyl or propargyl group. These include biotin-modified cryptophane biosensors for detecting streptavidin,[30−34] an enzyme-responsive biosensor for matrix metalloproteinase-7 (MMP-7),[35] and a series of benzenesulfonamide-functionalized cryptophane-A derivatives that exhibited isozyme-specific chemical shift changes, upon binding carbonic anhydrases I or II.[36] Another example included a peptide-labeled $^{129}$Xe biosensor by Schlundt et al. that produced a 1 ppm downfield shift upon binding to a major histocompatibility complex (MHC) class II protein.[37] The delivery of cryptophanes using cell-penetrating peptides or targeting cell-surface $\alpha_v\beta_3$ integrin receptors has also been demonstrated with cancer and normal cell lines.[38,39] Recent efforts have highlighted the potential for using xenon biosensors in cellular HP $^{129}$Xe magnetic resonance spectroscopy and imaging.[34,40−42]

**Received:** October 13, 2014
**Published:** December 1, 2014

   dx.doi.org/10.1021/bc5005526 | *Bioconjugate Chem.* 2015, 26, 101−109

**Scheme 1. Five-Step Synthesis of [2-(Trimethylsilyl)ethoxy]-2-*N*-[2-(trimethylsilyl)-ethoxycarbonyl]folic Acid**

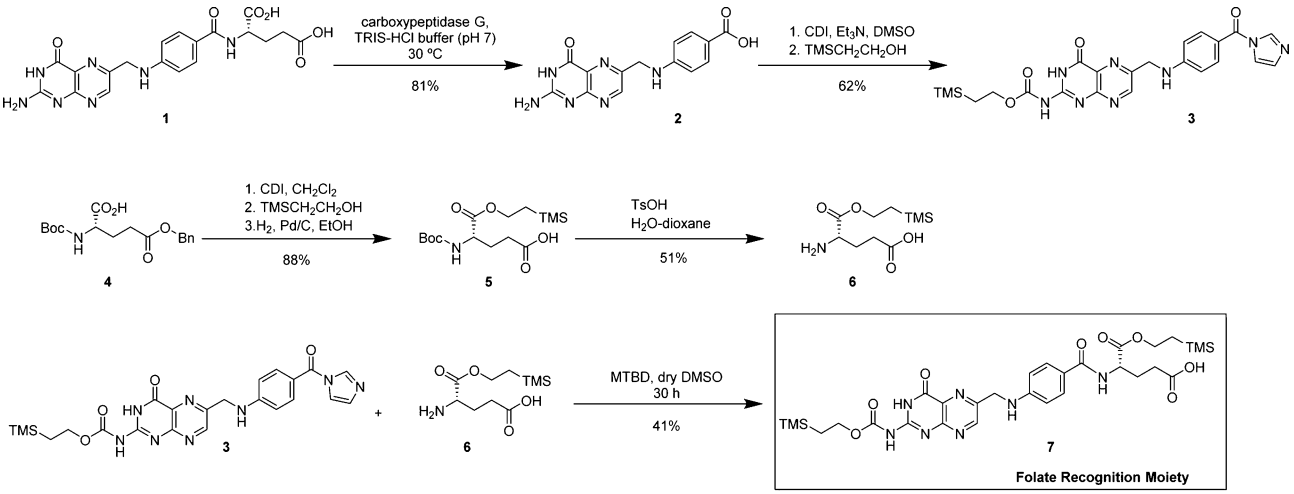


**Scheme 2. Synthesis of Unlabeled and Cy3-Labeled Biosensors 24 and 25, Respectively**[a]

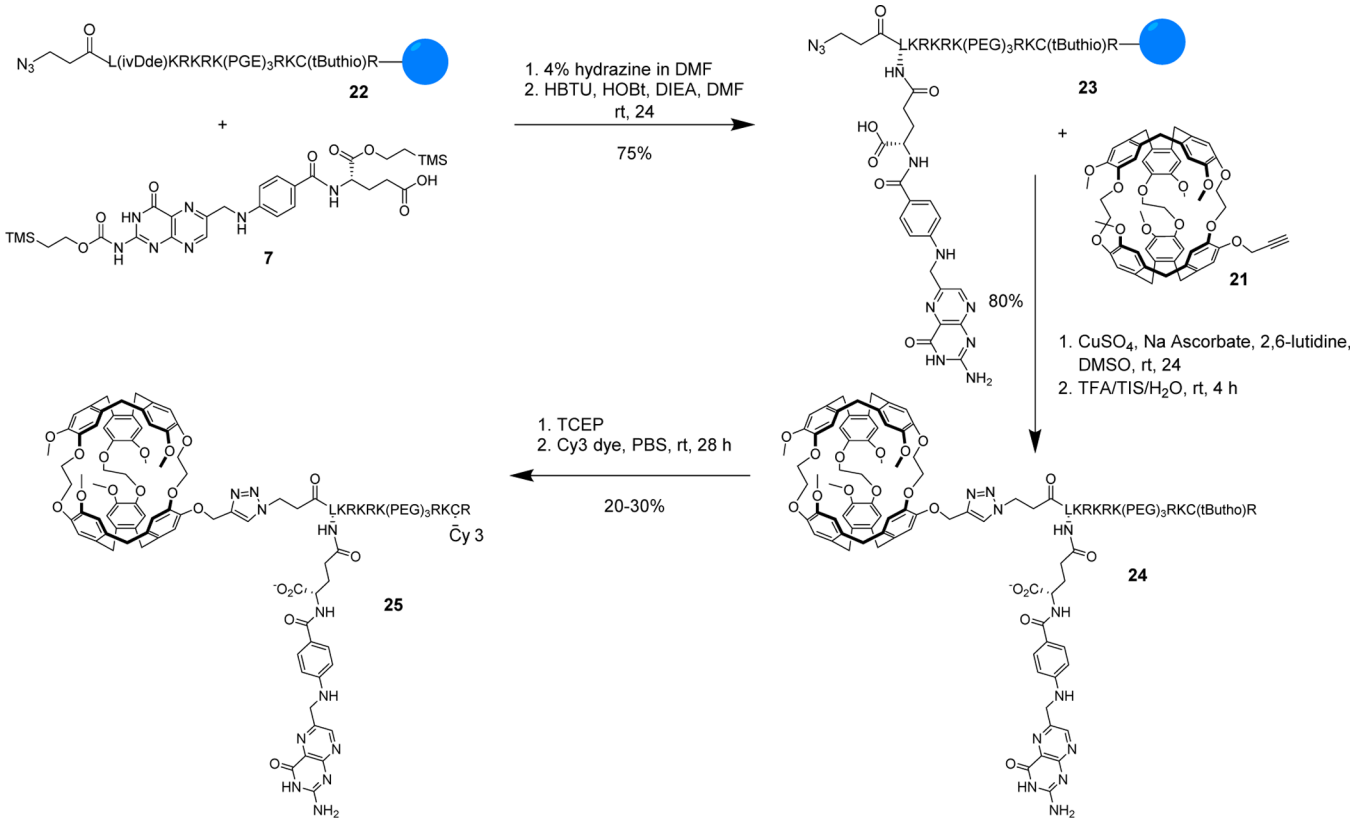


[a]Monopropargyl cryptophane was joined to the folate-conjugated azidopeptide on solid support via Cu(I)-catalyzed [3 + 2] azide−alkyne cycloaddition.

Folic acid has been investigated over the past two decades as a means for targeted delivery of payloads to tumor cells. In cells, there are three types of transporters that are responsible for the uptake of folate. These include reduced folate carrier (RFC),[43] proton-coupled high affinity folate transporter,[44] and folate receptor (FR, also known as high affinity folate binding protein).[45] Folate receptors are cell surface glycosylphosphatidylinositol (GPI)-linked membrane glycoproteins with molecular weights ranging from 38 to 45 kDa.[46] RFC is ubiquitously expressed throughout normal adult tissue, but as the name implies, this low affinity folate carrier is specific for the physiological form of reduced folic acid, 5-methyl tetrahydrofolate, which binds RFC with a micromolar dissociation constant. The high affinity FR ($K_d \approx 0.1-1$ nM, 1:1 stoichiometry) binds the nonphysiological folic acid as well as 5-methyltetrahydrofolate. FR exhibits narrow tissue distribution, being predominately expressed on the apical surface of polarized epithelial cells and thus not in contact with circulating folate. In humans, FR has 4 different isoforms: $\alpha$, $\beta$, $\gamma$, and $\delta$, where $\alpha$ and $\beta$ are membrane-bound.[45] Among them, FR$\alpha$ is overexpressed in non-mucinous adenocarcinomas of the ovary, cervix, uterus, and ependymal brain tumors;[45,47,48] FR$\alpha$ is


dx.doi.org/10.1021/bc5005526 | Bioconjugate Chem. 2015, 26, 101−109

overexpressed in 90% of ovarian carcinomas; and higher levels of expression are generally associated with poorly differentiated and aggressive tumors.[49,50] It is believed that FR$\alpha$ is overexpressed because the fast growth rate of cancer cells requires more folic acid.[45] FR expression is generally absent from normal tissues except in the choroid plexus, the placenta, and at low levels in lung, thyroid, and kidney. These FRs do not present a problem when using folic acid to target cancer because of localizations inaccessible to circulation; the brain side of the blood-brain barrier (choroid plexus), on the luminal side (lungs and gut), and in the proximal tubule lumen (kidney). FR functions via receptor-mediated endocytosis. FR is largely recycled back to the cell surface. Additionally, folate remains stable for several hours after endocytosis by cancer cells.[51] These characteristics make FR$\alpha$ an attractive target for the development of a new cryptophane biosensor. Here, we explored bioconjugation strategies for synthesizing a folate−cryptophane biosensor that targets cancer cells overexpressing FR$\alpha$.

The FR−cryptophane biosensor was designed with four functional components: First was a monopropargyl derivative of cryptophane-A, which is known to bind xenon in organic and aqueous solvents.[25,26,29,52] Second was a solubilizing polycationic (RKR-repeat) peptide where the positive charges were deliberately interrupted by a polyethylene glycol (PEG) unit: This avoided the problem that polycationic sequences of five or more peptide units can induce nonspecific cell uptake.[53] Third, a folate-linker moiety with high affinity for FR$\alpha$ was synthesized and conjugated via an orthogonally protected lysine on the peptide sequence. This final synthetic step involved reaction of the N-terminal azide of the peptide-folate conjugate with monopropargyl cryptophane via Cu(I)-catalyzed [3 + 2] azide−alkyne cycloaddition (CuAAC).[54−56] Finally, a Cy3 fluorescent dye was conjugated via maleimide linkage to a cysteine residue on the peptide. The dye assisted in fluorescence imaging and quantitation of biosensor uptake in both FR+ and FR− cells. Cell uptake and cytotoxicity studies were performed using a combination of confocal laser scanning microscopy, flow cytometry, and MTT assays for FR+ and FR− cancer cells.

## RESULTS AND DISCUSSION

**Synthesis and Characterization of Folate−Cryptophane Conjugate.** The fluorescent, folate−cryptophane conjugate was synthesized in 20 nonlinear steps from four commercially available starting materials. Folate recognition moiety **7** (5 steps, Scheme 1), monopropargyl cryptophane **21** (12 steps), and solubilizing azido-peptide **22** were joined in two steps to form biosensor **24** and finally conjugated with Cy3 dye (1 step) to give the fluorescent biosensor **25** (Scheme 2).

**Synthesis of $\alpha$-[2-(Trimethylsilyl)ethoxy]-2-*N*-[2-(trimethylsilyl)-ethoxycarbonyl] Folic Acid (7).** Folic acid has two carboxylates ($\alpha$- and $\gamma$-) whose reaction with the peptide sequence via *N*,*N*′-dicyclohexylcarbodiimide (DCC) would produce a mixture of $\alpha$-folate and $\gamma$-folate conjugates. Because only the $\gamma$-conjugate is recognized by the FR$\alpha$ receptor, a selectively protected folic acid derivative **7** was synthesized in 5 nonlinear steps in 13% overall yield following established protocols (Scheme 1).[57] The folate recognition moiety was prepared from two intermediates: the 2-*N*-teoc-pteroic acid derivative, where teoc is 2-(trimethylsilyl)-ethoxycarbonyl), and the $\alpha$-carboxyl-protected glutamic acid.[57] Folic acid **1** underwent enzymatic hydrolysis with carboxypeptidase-G to give pteroic acid **2**. Carbonyldiimidazole (CDI) and 2-trimethylsilylethanol in dry dimethyl sulfoxide (DMSO) were added to the crude pteroic acid to produce the protected pteroic acid, 1-(2-*N*-teoc-pteroyl)imidazole **3** in 62% yield. In order to synthesize the second intermediate, the $\alpha$-carboxylate group in *N*-Boc-L-Glu (OBn)-OH **4** was protected by treating it with CDI and 2-trimethylsilylethanol while the $\gamma$-carboxylate group was selectively deprotected using Pd−C to give **5** in 88% yield. The *N*-Boc protecting group was subsequently removed using TsOH to give $\alpha$-(2-TMS-ethyl) glutamate **6** in 51% yield. Finally, **3** was treated with 1.5 equiv of **6** and *N*-methyl-1,5,9-triazabicyclo[4.4.0]-decene (MTBD) in dry DMSO to give the folate recognition moiety **7** (41% yield).

**Monopropargyl Cryptophane (21).** A monopropargyl derivative of cryptophane-A was synthesized in 12 nonlinear steps in 3% overall yield (Supporting Information, Schemes S1−S3).[35]

**Synthesis of Fluorescent Folate−Cryptophane Conjugate (25).** Final steps in biosensor synthesis are shown in Scheme 2. The azidopeptide **22** was synthesized by standard solid-phase synthesis using Fmoc-substituted reagents in 85% yield and consisted of three polyethylene glycol units and lysine-arginine units to help solubilize the cryptophane in water.[58] 3-Azido propionic acid was prepared according to literature procedures and incorporated as the N-terminal residue.[59] The cysteine was incorporated in the peptide to enable site-specific fluorescent labeling of the biosensor for cell studies. The azidopeptide was orthogonally deprotected using 4% hydrazine in water and readily coupled to the $\gamma$-folate conjugate **7** in dry DMF to yield **23** in 75% yield. In order to monitor the reaction, a portion of the reaction mixture was cleaved from the resin and purified by reverse-phase HPLC. Once product formation was confirmed, **23** (still on solid support) was coupled to monopropargyl cryptophane **21** to give **24** by copper(I)-catalyzed [3 + 2] cycloaddition. Although the yield for **24** was initially low (~20%), it was subsequently improved to approximately 80% by using a large excess of sodium ascorbate (40 equiv) to ensure that copper remained reduced as Cu(I) to catalyze the reaction. The product was cleaved from solid support, purified by reverse-phase HPLC and was determined to be readily soluble in water. To fluorescently label the conjugate **24**, the cysteine was deprotected using TCEP and coupled with the maleimide-functionalized Cy3 dye ($\lambda_{ex}$ = 550 nm, $\lambda_{em}$ = 575 nm). **25** was purified by reverse-phase HPLC. Cy3 labeling efficiencies were determined from the ratio of dye absorbance at 550 nm ($\varepsilon_{550}$ = 150 000 $M^{-1}$ $cm^{-1}$ with a correction factor of 0.05 at $A_{280}$) to the cryptophane absorbance at 280 nm ($\varepsilon_{280}$ = 10 000 $M^{-1}$ $cm^{-1}$).[60] Cy3-labeling yields were only 20−30%, likely a result of steric hindrance from both the bulky cryptophane and folate group appended to the peptide. Removal of excess TCEP using a gel filtration column, prior to Cy3 addition, did not improve the yield.

**Visualization of Cell Delivery by Confocal Microscopy.** In order to determine whether **25** could be selectively delivered to FR+ cells, confocal laser scanning microscopy (CLSM) was performed as shown in Figure 1. Human nasopharyngeal epidermoid carcinoma cells (KB) and human cervical carcinoma cells (HeLa) were used as receptor positive cell lines, with KB strongly overexpressing FR$\alpha$ and HeLa moderately expressing FR$\alpha$.[61] Human fibrosarcoma (HT-1080) was used as a negative control cell line (FR−) because


dx.doi.org/10.1021/bc5005526 | Bioconjugate Chem. 2015, 26, 101−109

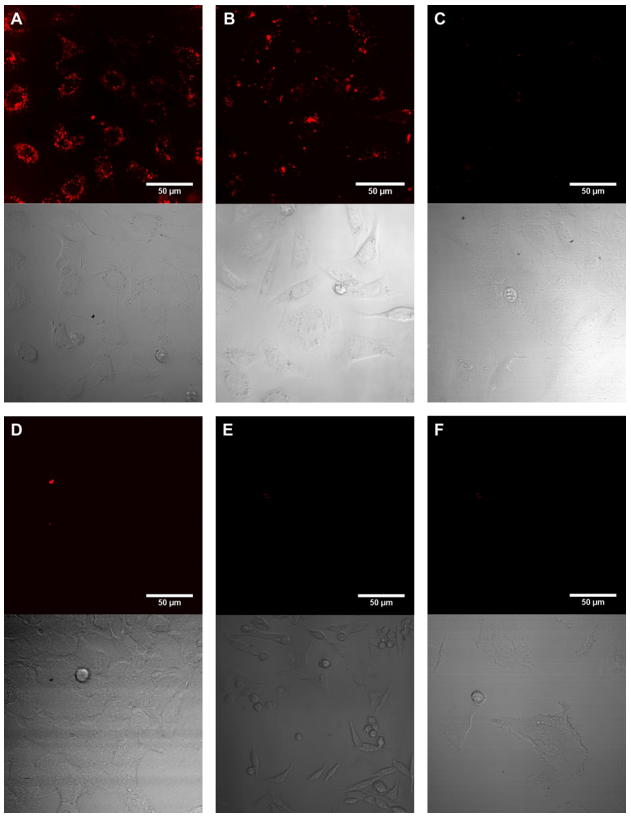


**Figure 1.** Confocal micrographs and corresponding brightfield images of 4 $\mu$M Cy3-labeled biosensor **25** targeting FR$\alpha$. Uptake occurred in (A) KB, (B) HeLa, and (C) HT-1080 cells after 4 h incubation at 37 °C in folic acid-depleted media. Uptake was blocked in (D) KB, (E) HeLa, and (F) HT-1080 cells preincubated in folic acid containing media.

these cells exhibit relatively little folate uptake.[62] After 4 h incubation with Cy3-labeled **25**, fluorescence was seen evenly distributed in the perinuclear region of KB cells as expected for receptor-mediated endocytosis (Figure 1A). This was desirable as nuclear internalization of imaging agents can cause potential mutagenic effects on healthy cells. Uptake of Cy3-labeled **25** in HeLa cells was also confirmed by CLSM after 4 h incubation (Figure 1B). The fluorescence intensity was lower in HeLa cells than in KB cells, which was in agreement with previous studies.[61,62] Uptake of **25** was negligible in HT-1080 (FR−) cells, thereby indicating that biosensor **25** was able to discriminate between FR+ and FR− cells (Figure 1C). To analyze whether the uptake of **25** was facilitated by folate receptor-mediated endocytosis, **25** was coincubated with folic acid rich medium for all three cell lines. Because folic acid is known to have a very high affinity for FR$\alpha$, excess folic acid was expected to outcompete **25**, thereby blocking uptake. The reduction in fluorescence in Figure 1D−F indicated that **25** was specifically recognized by the FR receptor. Indeed, the folate recognition moiety was critical for cellular uptake of this biosensor.

**Cytotoxicity Studies.** The cytotoxicity of folate−cryptophane conjugate **24** was evaluated by incubating KB (FR+) and HT-1080 (FR−) cells with increasing concentrations (0 to 100 $\mu$M) of **24** for 24 h, as shown in Figure 2. In KB cells, the viability (scaled to 100% at 0 $\mu$M) decreased from 80% at 10 $\mu$M to 50% at 38 $\mu$M. Maximum toxicity in KB cells (23% viability) was found when the cells were incubated with the

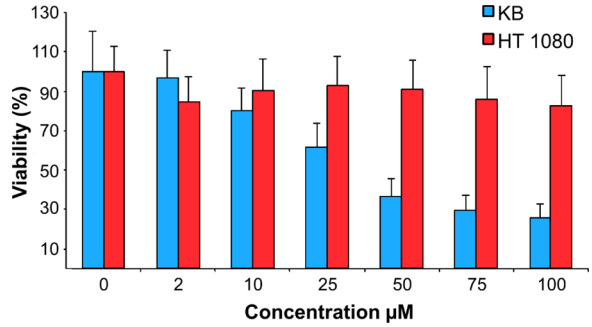


**Figure 2.** Cytotoxicity assays for folate-conjugated cryptophane **24** in KB (blue) and HT-1080 cells (red). Percent viability was determined via MTT assay after 24 h incubation with increasing concentrations of **24** as compared to untreated cells.

highest concentration of **24** (100 $\mu$M). Cell viabilities determined when 0−10 $\mu$M of the biosensor was added to KB cells were comparable to those seen previously with fluorescent contrast agents such as folate-substituted poly(*p*-phenyleneethynylene).[63] At concentrations ~2 $\mu$M, **25** exhibited sufficient fluorescence intensity to be detected intracellularly via both confocal microscopy and flow cytometry and was also minimally cytotoxic. The viability of HT-1080 cells with **24** ranged from 100% at 0 $\mu$M to 82% at 100 $\mu$M. The greater cytotoxicity observed for KB cells was likely due to the higher levels of FR$\alpha$ that are expressed on KB cells versus HT-1080 cells, which in turn caused increased intracellular accumulation of the folate−cryptophane conjugates. Similar trends were seen in a previous study where a cyclic RGD peptide-conjugated cryptophane was determined to be more toxic in cell lines overexpressing the targeted $\alpha_v\beta_3$ integrin receptors (60% toxicity in ASPC-1 cells versus 30% toxicity in HFL-1 cells) after 24 h incubation at 100 $\mu$M concentration.[39]

**Quantifying Cellular Internalization with Flow Cytometry.** In an effort to quantify the selective cellular internalization of **25** in KB and HT-1080 cells, flow cytometry was performed (Figure 3). After 4 h incubation in both KB and

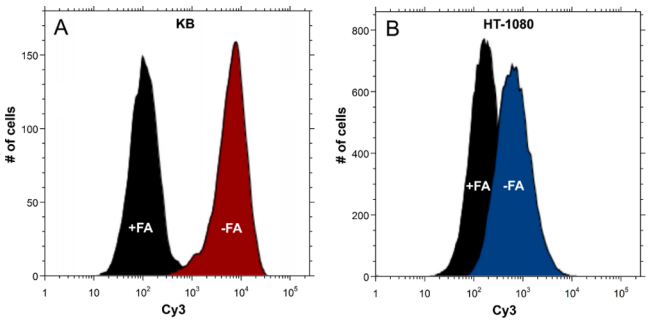


**Figure 3.** Flow cytometry quantified cell uptake of 4 $\mu$M Cy3-labeled **25**. Uptake in (A) KB (FR+, red) and (B) HT-1080 (FR-, blue) cells was compared to cells inhibited by folic acid (black).

HT-1080 cells, there was a dramatic increase in cell-associated fluorescence. When biosensor **25** was coincubated with excess folic acid, the increase in median fluorescence intensity was much lower than when folic acid was absent. This was in agreement with the results from the CLSM studies, where uptake was significantly reduced when excess folic acid was present. In the absence of folic acid, the median cell-associated fluorescence intensity was approximately 45-fold higher in KB


dx.doi.org/10.1021/bc5005526 | *Bioconjugate Chem.* 2015, 26, 101−109

cells and 3-fold higher in HT-1080 cells. Based on flow cytometry data, it was determined that the median fluorescence intensity in KB cells was approximately 10-fold higher than in HT-1080 cells, consistent with the expected levels of FR$\alpha$ expression.[62,64] These data confirmed that **25** selectively targeted cancer cells overexpressing the intended folate receptors.

**Hyperpolarized $^{129}$Xe NMR.** Hyperpolarized $^{129}$Xe NMR spectra of **24** were acquired at 60 $\mu$M in acetate buffer at pH 5.0 using a 10 mm NMR probe and BURP-shaped soft pulse. Sample temperature was controlled by a VT unit on the NMR spectrometer to 300 ± 1 K. Chemical shifts were referenced relative to $^{129}$Xe gas at 0 ppm when extrapolated to 0 atm.

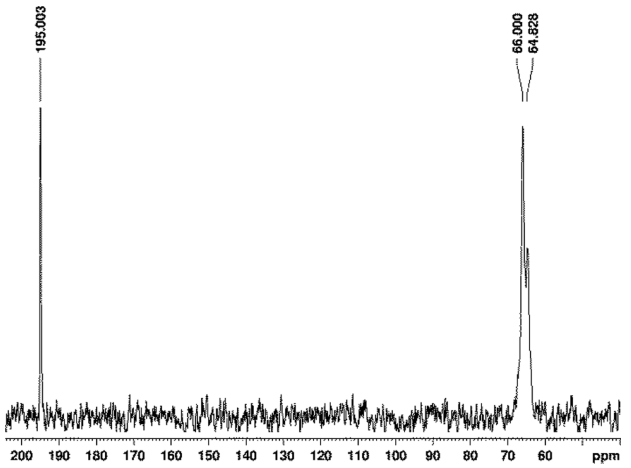


**Figure 4.** Hyperpolarized $^{129}$Xe NMR spectrum of 60 $\mu$M **24** in acetate buffer at pH 5.0 (40 scans; $S/N$ = 30:1 with 50 Hz line broadening).

Figure 4 shows a HP $^{129}$Xe-aq NMR peak at 195.0 ppm and $^{129}$Xe NMR chemical shifts of 64.8 and 66.0 ppm corresponding to diastereomers of **24**. This was due to the chirality of the three components—folate, peptide, and cryptophane (LRL and LRR). Cryptophane-A is a chiral molecule and the racemic mixture of two enantiomers encapsulating xenon is known to give rise to a single $^{129}$Xe NMR resonance in water.[65] However, upon conjugation of chiral moieties to racemic cryptophane, diastereomers are formed. Previous examples of xenon biosensor diastereomers include the biotin-conjugated cryptophane developed by Spence et al.[30] The biosensor consisted of four diastereomers due to the chiral cryptophane, L-amino acids, and maleimide center formed when the biotin was conjugated to the rest of the biosensor (RLR, RLL, LLR, LLL).[30] This resulted in 4 distinct peaks in the $^{129}$Xe NMR spectrum. Similarly, the enzyme MMP-7 biosensor developed in our laboratory indicated the presence of two diastereomers that were separated by 0.6 ppm.[35] This was due to the chirality of the two components, peptide and cryptophane-A (RL and LL).[35,52,65]

Our HP $^{129}$Xe NMR studies with folate binding protein (FBP) and **24** resulted in no observable protein bound signal (Supporting Information, Figure S11). FBP is a membrane-bound protein and is known to aggregate at low micromolar concentrations.[66] It was necessary, therefore, to investigate experimental conditions where the protein is maximally stable (30 $\mu$M FBP, 30 and 60 $\mu$M biosensor **24** in acetate buffer, pH 5.0 with and without 10% glycerol; vortex mixed and incubated 30 min). The $^{129}$Xe NMR peaks for **24** in the presence of FBP (at 66.7 and 68.0 ppm, Figure S11) were essentially identical to those shown for **24** in the absence of FBP (Figure 4). However, it is important to emphasize that the biosensor need not induce a chemical shift change to be useful *in vivo*. As we have demonstrated with the confocal microscopy and flow cytometry studies, the biosensor should preferentially localize in FR+ cells as the free biosensor is diluted in circulation. Thus, detection of HP $^{129}$Xe NMR signal corresponding to the cryptophane biosensor will indicate FR+ tissue. Recent improvements in $^{129}$Xe hyperpolarization methods and HP $^{129}$Xe cellular NMR techniques should make it possible using similar folate-cryptophane biosensors in the future to discriminate between FR+ and FR− cells by $^{129}$Xe NMR.[34,41,67]

## CONCLUSIONS

In summary, a water-soluble, folate- and Cy3-conjugated cryptophane biosensor was synthesized in 20 nonlinear steps and fully characterized. During conjugation, the folate moiety was selectively protected to ensure that only the $\alpha$-carboxylate group was available to bind to FR$\alpha$. Confocal imaging with FR+ and FR− cells confirmed the selective uptake of biosensor via folate receptor-mediated endocytosis by cells overexpressing FR$\alpha$. Flow cytometry analysis quantified that uptake was 45-fold higher in KB cells and 3-fold higher in HT-1080 cells than when competing excess folate was in solution. Also, the median fluorescence intensity was approximately 10-fold higher in KB cells than HT-1080 cells, which motivates the use of folate-conjugated cryptophane for *in vivo* biosensing in cells overexpressing FR$\alpha$. Cytotoxicity assays indicated that in the relevant concentration range required for confocal and flow cytometry analysis (1−10 $\mu$M), the viability was greater than 80% in both cell lines. Further advances in efficient cryptophane synthesis[68,69] will make it more practical in the future to generate folate-cryptophane biosensors in larger quantities needed for cell or *in vivo* $^{129}$Xe NMR studies.

## EXPERIMENTAL PROCEDURES

**Reagents.** *Sigma-Aldrich.* Dimethyl sulfoxide (DMSO), dimethylformamide (DMF), folate binding protein (FBP), folic acid, methanol, triisopropylsilane (TIPS, 99%), 2,6-lutidine, piperidine, 3-(4,5- dimethyl-2-thiazolyl)-2,5-diphenyl-2*H*-tetrazolium bromide (MTT).

*Fisher.* Sodium chloride, copper(II) sulfate, trifluoroacetic acid (TFA), diethyl ether ($Et_2O$).

*Alfa Aesar.* Cesium carbonate, L-glutathione.

*Novabiochem.* 2-(1*H*-benzotriazole-1-yl) 1,1,3,3-tetramethyluronium hexafluorophosphate (HBTU), *N*-hydroxybenzotriazole (HOBt), *N*-methylmorpholine (0.4 M), Fmoc-15-amino-4,7,10,13 tetraoxapentadecanoic acid ($(PEG)_3$), rink amide resin, Fmoc-protected amino acids including Fmoc-L-Lys(ivDde)-OH, Fmoc-L-Lys(Boc)-OH, Fmoc-L-Arg(Pbf)-OH, Fmoc-Cys(tButhio)-OH, *N*-methylmorpholine (0.4 M).

*GE Healthcare.* Cy3 monoreactive dye pack.

*Calbiochem.* Tris(2-carboxyethyl)phosphine hydrochloride (TCEP-HCl).

*Invitrogen.* RPMI-1640 medium, folate-depleted RPMI-1640 medium, Dulbecco's phosphate buffered saline (DPBS).

For biological assays, all solutions were prepared using deionized water purified by Mar Cor Premium grade Mixed Bed Service Deionization.


dx.doi.org/10.1021/bc5005526 | *Bioconjugate Chem.* 2015, 26, 101−109

**General Methods.** All organic reactions were carried out under nitrogen atmosphere. $^{1}$H NMR (500.14 MHz) and $^{13}$C NMR (125.77 MHz) spectra were obtained on a Bruker AMX 500 spectrometer at the University of Pennsylvania Chemistry Department NMR facility. Electrospray ionization (ESI) mass spectrometry was performed in low-resolution mode on a Micromass LC Platform and in high-resolution mode on a Micromass Autospec. Matrix-assisted laser desorption/ionization mass spectrometry (MALDI-MS) was performed on a Bruker Daltonic Ultraflex III MALDI-TOF/TOF spectrometer at the Mass Spectrometry Center in the Chemistry Department at the University of Pennsylvania. Column chromatography was performed using 60 Å porosity, 40−75 μm particle size silica gel from Sorbent Technologies. Thin layer chromatography (TLC) was performed using silica gel plates with UV light at 254 nm for detection. HPLC analysis was performed on an Agilent 1100 system equipped with a quaternary pump and diode array detector using a Varian Microsorb-MV 300−5 C8 column (4.6 × 250 mm, 5 μm). The gradient eluent was composed of two solvents: 0.1% aqueous TFA (solvent A) and a 0.1% solution of TFA in $CH_3CN$ (solvent B). UV−visible spectra were measured using a diode-array Agilent 89090A spectrophotometer.

**Synthesis of 7.** α-[2-(Trimethylsilyl)ethoxy]-2-*N*-[2-(trimethylsilyl)-ethoxycarbonyl]folic acid (**7**) was prepared according to literature procedures[57] (Scheme 1) and matched the reported physical constants and NMR spectra (SI, Figures S1 and S2).

**Synthesis of 21.** Monopropargyl cryptophane was prepared according to literature procedures[35] and matched the reported physical constants and NMR spectra.

**Synthesis of 22.** Peptide **22** (Scheme 2) was prepared by solid-phase synthesis using standard Fmoc amino acid protection chemistry on Rink Amide resin (0.1 mmol scale). Couplings of Fmoc-protected amino acids to the resin were carried out with HBTU and *N*-methylmorpholine to generate the activated ester. The resin was swelled in DMF (10 min) prior to synthesis. Amino acids were then added sequentially until 3-azidopropionic acid was attached at the N-terminus as the final step. All residues were coupled onto resin by the following procedure: removal of Fmoc group (20% piperidine solution in DMF, 2 × 5 min), wash (DMF, 6 × 30 s), activation (amino acid/HBTU/*N*-methylmorpholine, 1 × 30 s), coupling (amino acid/HBTU/*N*-methylmorpholine, 1 × 60 min), rinse (DMF, 3 × 30 s). The resin was swelled in DMF for 10 min and the orthogonal lysine was deprotected by washing the resin five times with 4% hydrazine in DMF. The resin was dried and the peptide was cleaved using a mixture of TFA, TIPS, and water (90/5/5) at rt for 4 h. The reaction mixture was filtered using a peptide vessel, concentrated and the peptide was precipitated by the addition of ether. The cleavage cocktail removed side chain protecting groups from all amino acids except for the *t*-butylthiol-protected cysteine. Semipreparative HPLC purification of **22** was accomplished using the following gradient: time 0, A/B = 95/5; 0−45 min, linear increase to A/B = 50/50; 45−47 min, linear increase to A/B = 20/80; 47−56 min, linear change to A/B = 20/80; 56−57 min, linear increase to A/B = 95/5; 57−72 min, linear change to A/B = 95/5 (SI, Figure S3). MALDI-MS calculated for peptide **22**, $C_{72}H_{141}N_{31}O_{16}S_2$ (M + $H^+$) 1761.06; found 1760.91 (SI, Figure S4).

**Synthesis of 23.** Peptide **22** on the Rink Amide resin (30 mg, maximum, 0.0201 mmol azidopeptide **22**, 1 equiv) was allowed to swell in DMF (500 μL) in a 10 mL peptide vessel for 10 min. The solution was filtered and 1 mL of 4% hydrazine in DMF was added to deprotect the ivDde group on the orthogonally protected lysine. This was repeated 5 times and the absorption of the filtrate at 290 nm was monitored by UV−vis spectroscopy to ensure that deprotection had taken place. The resin was dried under vacuum. **22** was then added to a mixture of **7** (0.0402 mmol, 2 equiv), HBTU (0.0603 mmol, 3 equiv), HOBt (0.0905 mmol, 4.5 equiv), and DIEA (0.1206 mmol, 6 equiv) in dry DMF. The reaction was stirred overnight at rt under nitrogen. Once the reaction was complete, the resin was carefully transferred to a fritted reaction vessel and washed sequentially with DMF, $CH_2Cl_2$, MeOH, 1:1 MeOH/$CH_2Cl_2$, and MeOH before drying under vacuum. The peptide coupled to folate **23** was cleaved from the resin using a mixture of TFA, TIPS, and water (90/5/5) at rt for 4 h. The reaction mixture was filtered using a peptide vessel, concentrated, and the peptide was precipitated by the addition of ether. The cleavage cocktail removed side chain protecting groups from all amino acids except for the *t*-butylthiol-protected cysteine. Semipreparative HPLC purification of **23** was accomplished using the following gradient: time 0, A/B = 95/5; 0−45 min, linear increase to A/B = 50/50; 45−47 min, linear increase to A/B = 20/80; 47−56 min, linear change to A/B = 20/80; 56−57 min, linear increase to A/B =95/5; 57−72 min, linear change to A/B = 95/5 (SI, Figure S5). MALDI-MS calculated for peptide−folate conjugate **23**, $C_{91}H_{158}N_{38}O_{21}S_2$ (M + $H^+$) 2184.19; found 2184.05 (SI, Figure S6).

**Synthesis of 24.** Monopropargyl cryptophane **21** (20 mg, 0.02186 mmol, 2 equiv) in 900 μL dry DMSO was added to **23** (18.2 mg on solid support, maximum 0.01093 mmol azidopeptide, 1 equiv) and allowed to stir for 10 min. 2,6-Lutidine (0.0219 mmol, 1 equiv) was added and the reaction mixture was degassed. Sodium ascorbate (0.4372 mmol, 40 equiv) was added dropwise, the mixture was degassed, and finally an aqueous solution of copper(II) sulfate (0.0054 mmol, 0.5 equiv) was added. The suspension was degassed with $N_2$ and stirred at rt for 24 h. The resin was then carefully transferred to a fritted reaction vessel and washed sequentially with $CH_2Cl_2$, MeOH, water, and 1:1 MeOH/$CH_2Cl_2$ before drying under vacuum. The [3 + 2] cycloaddition reaction between the azide-terminated folate-peptide **23** and monopropargyl cryptophane **21** generated the folate-peptide-cryptophane conjugate **24** which was cleaved from the resin using a mixture of TFA, TIPS, and water (90/5/5) at rt for 4 h. The reaction mixture was filtered using a peptide vessel, concentrated, and the peptide was precipitated by the addition of ether. The cleavage cocktail removed side chain protecting groups from all amino acids except for the *t*-butylthiol-protected cysteine. Semipreparative HPLC purification of **24** was accomplished using the following gradient: time 0, A/B = 95/5; 0−65 min, linear increase to A/B = 30/70; 65−68 min, linear increase to A/B = 20/80; 68−70 min, linear increase to A/B = 5/95 (SI, Figure S7). MALDI-MS calculated for **24**, $C_{147}H_{211}N_{38}O_{32}S_2$ (M + $H^+$) 3102.61; found 3103.08 (SI, Figure S8).

**Synthesis of 25.** Cys-protected folate-peptide-cryptophane conjugate **24** was dissolved in PBS buffer (100 mM, pH 7.1) at a concentration of 60 μM. The GE protocol was followed to deprotect the *t*-butylthiol group and label the cysteine with the Cy3-maleimide construct. TCEP (0.0006 mmol, 10 equiv) was added to a 1 mL PBS solution containing **24** and degassed. The solution was stirred for 40 min to which was added Cy3 dye


dx.doi.org/10.1021/bc5005526 | *Bioconjugate Chem.* 2015, 26, 101−109

dissolved in 50 μL dry DMSO. The reaction was degassed and stirred under nitrogen at rt for 16 h. The reaction mixture was purified by HPLC using the following gradient: time 0, A/B = 95/5; 0−65 min, linear increase to A/B = 30/70; 65−68 min, linear change to A/B = 20/80; 68−70 min, A/B = 5/95 (SI, Figure S9). MALDI-MS calculated for $C_{180}H_{253}N_{42}O_{42}S_3$ ($M+H^+$) 3771.81; found 3771.59 (SI, Figure S10). Extinction coefficients used to determine solution concentrations of Cy3-labeled **25** were $\varepsilon_{280}$ = 38 000 $M^{-1}$ $cm^{-1}$ and $\varepsilon_{552}$ = 150 000 $M^{-1}$ $cm^{-1}$ in water.

**Cell Culture.** KB, HeLa, and HT-1080 cells were obtained from Dr. Jerry Glickson (University of Pennsylvania, Perelman School of Medicine, Philadelphia, PA). All cells were grown in 25 $cm^2$ tissue culture flasks in RPMI-1640 with 25 mM HEPES supplemented with 2 mM L-glutamine, 15% fetal calf serum, 100 units penicillin, and 100 units streptomycin. Cells were subcultured on a weekly basis.

**Cell Viability (MTT) Assay.** In 96 well plates 25 000 KB or HT-1080 cells were plated per well and allowed to grow overnight. A stock solution of nonfluorescently labeled folate-peptide-cryptophane conjugate **24** was added to wells in triplicate at final concentrations of 0, 2, 10, 25, 50, 75, and 100 μM and incubated for 24 h in the dark. The medium was aspirated and the cells were washed thrice with DPBS before being treated with 20 μL of MTT (5 mg/mL) for 3 h. The medium was removed and DMSO was added to solubilize the resulting crystals. A Labsystems Fluoroskan II microplate reader was used to record the absorbance at 540 nm. Absorbance readings were subtracted from the value of wells containing untreated cells, and the reduction in cell growth was calculated as a percentage of control absorbance in the absence of any treatment. Data show the mean of at least three independent experiments ± SD.

**Cell Uptake Studies.** KB, HeLa, and HT-1080 cells were grown to confluence on LabTek 8-well microscope slides with glass coverslip bottoms at a density of 50 000 cells per plate. The cells were grown in folate-depleted media for 24 h prior to incubation with 4 μM solution of Cy3-labeled **25** for 4 h at 37 °C. For blocking studies, cells were grown in media containing folic acid for 24 h prior to incubation with **25** under the same conditions mentioned above. The medium was removed and the cells were washed three times with DPBS. Cells were visualized using an Olympus FV1000 confocal laser scanning microscope with 543 nm (HeNe) laser excitation and Cy3 emission filter under 40× magnification (Olympus UApo/340, 1.15 NA water objective).

**Flow Cytometry Experiments.** KB and HT-1080 cells were seeded in T25 flasks each containing $10^6$ cells and grown for 1 day in folate-depleted RPMI-1640 medium. The cells were incubated for 4 h with 4 μM **25** (1.3 mL/flask). For blocking studies, 4 μM **25** was added in the presence of medium containing folic acid. The medium was aspirated and cells washed 3 times with 2 mL PBS. The cells were detached using trypsin-EDTA and centrifuged. The supernatant was aspirated and resuspended in 650 μL 10% FBS in Dulbecco's PBS and immediately analyzed on a BD LSRII machine at the Flow Cytometry Laboratory, Abramson Cancer Center, at the University of Pennsylvania.

**$^{129}$Xe NMR.** Hyperpolarized $^{129}$Xe was generated using a home-built $^{129}$Xe hyperpolarizer, which is based on the formerly commercially available Nycomed-Amersham (now GE) IGI.Xe.2000 system. A gas mixture of 10% $N_2$, 89% He, and 1% natural abundance Xe (Spectra Gases) was flowed through the hyperpolarizer. $^{129}$Xe was hyperpolarized to 10−15% after having been cryogenically separated, accumulated, thawed, and collected in CAV NMR tubes (New Era). After Xe collection, NMR tubes were shaken vigorously to mix cryptophane solutions with Xe. All $^{129}$Xe NMR measurements were carried out on a 500 MHz Bruker BioDRX NMR spectrometer. RF pulse frequency for $^{129}$Xe was 138.12 MHz. Samples were observed using a 10 mm PABBO NMR probe. $^{129}$Xe NMR spectra were acquired using the exchange signal averaging (ESA) method. 54 Selective pulses (90 degree flip angle, EBURP-1 shaped) were generated at the Xe@cryptophane resonance frequencies. Each pulse lasted 5 ms, which gave a designated excitation region 1 kHz (7.2 ppm). All spectra were signal averaged by 40 scans. A delay of 0.15 s was given between scans to allow polarized Xe to exchange in and depolarized Xe to exchange out of the cryptophane cavity. The natural line widths of Xe@cryptophane peaks are around 80 Hz (fwhm, Lorentzian fitted). The spectra shown above are exponentially broadened by 100 Hz, to give a larger signal/noise ratio. Sample temperature was controlled by a VT unit on the NMR spectrometer to 27 ± 1 °C.

## ■ ASSOCIATED CONTENT

### Supporting Information

HPLC, MALDI-MS, and NMR characterization. This material is available free of charge via the Internet at http://pubs.acs.org.

## ■ AUTHOR INFORMATION


### Corresponding Author

*E-mail: ivandmo@sas.upenn.edu. Phone: 215-898-6459.


### Notes

The authors declare no competing financial interest.

## ■ ACKNOWLEDGMENTS

We thank Dr. George Furst for assistance with NMR, Dr. Jerry Glickson for providing cell lines, and Dr. Qian Wei, Dr. Aru Hill, and Tara Kaufmann for their early contributions to this work. This research was supported by NIH CA110104, GM097478, and DOD BC061527. Bruker Ultraflex III MALDI-TOF/TOF and Waters LCT Premier XE LC/MS ESI-TOF were supported by NSF CHE-0820996 and NIH 1S10RR023444. Olympus FV1000 confocal microscope was supported by NIH 1S10RR021113.

## ■ REFERENCES

(1) Sharma, V., and Piwnica-Worms, D. (2002) Molecular imaging of gene expression and protein function *in vivo* with PET and SPECT. *J. Magn. Reson. Imaging 16* (4), 336−351.

(2) Degani, H., Gusis, V., Weinstein, D., Fields, S., and Strano, S. (1997) Mapping pathophysiological features of breast tumors by MRI at high spatial resolution. *Nat. Med. 3* (7), 780−782.

(3) Foster-Gareau, P., Heyn, C., Alejski, A., and Rutt, B. K. (2003) Imaging single mammalian cells with a 1.5 T clinical MRI scanner. *Magn. Reson. Med. 49* (5), 968−971.

(4) Moats, R. A., Fraser, S. E., and Meade, T. J. (1997) A "smart" magnetic resonance imaging agent that reports on specific enzymatic activity. *Angew. Chem., Int. Ed. Engl. 36* (7), 726−728.

(5) Mugler, J. P., III, Driehuys, B., Brookeman, J. R., Cates, G. D., Berr, S. S., Bryant, R. G., Daniel, T. M., de Lange, E. E., Downs, J. H., III, Erickson, C. J., Happer, W., Hinton, D. P., Kassel, N. F., Maier, T., Phillips, C. D., Saam, B. T., Sauer, K. L., and Wagshul, M. E. (1997) MR imaging and spectroscopy using hyperpolarized $^{129}$Xe gas: preliminary human results. *Magn. Reson. Med. 37* (6), 809−815.

(6) Golman, K., Zandt, R. I., Lerche, M., Pehrson, R., and Ardenkjaer-Larsen, J. H. (2006) Metabolic imaging by hyperpolarized $^{13}C$ magnetic resonance imaging for *in vivo* tumor diagnosis. *Cancer Res. 66* (22), 10855−10860.
(7) Hopkins, S. R., Levin, D. L., Emami, K., Kadlecek, S., Yu, J., Ishii, M., and Rizi, R. R. (2007) Advances in magnetic resonance imaging of lung physiology. *J. Appl. Physiol. 102* (3), 1244−1254.
(8) Cleveland, Z. I., Pavlovskaya, G. E., Elkins, N. D., Stupic, K. F., Repine, J. E., and Meersmann, T. (2008) Hyperpolarized Kr-83 MRI of lungs. *J. Magn. Reson. 195* (2), 232−237.
(9) Rider, O. J., and Tyler, D. J. (2013) Clinical implications of cardiac hyperpolarized magnetic resonance imaging. *J. Cardiovasc. Magn. Reson. 15*, 93.
(10) Nelson, S. J., Kurhanewicz, J., Vigneron, D. B., Larson, P. E., Harzstark, A. L., Ferrone, M., van Criekinge, M., Chang, J. W., Bok, R., Park, I., Reed, G., Carvajal, L., Small, E. J., Munster, P., Weinberg, V. K., Ardenkjaer-Larsen, J. H., Chen, A. P., Hurd, R. E., Odegardstuen, L. I., Robb, F. J., Tropp, J., and Murray, J. A. (2013) Metabolic imaging of patients with prostate cancer using hyperpolarized [1-$^{13}C$]pyruvate. *Sci. Transl. Med. 5* (198), 198ra108.
(11) Kurhanewicz, J., Vigneron, D. B., Brindle, K., Chekmenev, E. Y., Comment, A., Cunningham, C. H., Deberardinis, R. J., Green, G. G., Leach, M. O., Rajan, S. S., Rizi, R. R., Ross, B. D., Warren, W. S., and Malloy, C. R. (2011) Analysis of cancer metabolism by imaging hyperpolarized nuclei: prospects for translation to clinical research. *Neoplasia 13* (2), 81−97.
(12) Clever, H. L. (1979) *Krypton, Xenon, and Radon: Gas Solubilities*, Pergamon Press, Oxford.
(13) Tilton, R. F., and Kuntz, I. D. (1982) Nuclear magnetic-resonance studies of Xe-129 with myoglobin and hemoglobin. *Biochemistry 21* (26), 6850−6857.
(14) Robbins, T. A., Knobler, C. B., Bellew, D. R., and Cram, D. J. (1994) Host-guest complexion 0.67. A highly adaptive and strongly binding hemicarcerand. *J. Am. Chem. Soc. 116* (1), 111−122.
(15) Bartik, K., Luhmer, M., Heyes, S. J., Ottinger, R., and Reisse, J. (1995) Probing molecular cavities in alpha-cyclodextrin solutions by xenon NMR. *J. Magn. Reson., Ser. B 109* (2), 164−168.
(16) Fukutomi, J., Adachi, Y., Kaneko, A., Kimura, A., and Fujiwara, H. (2007) Inclusion complex formation of thiacalix[4]arene and Xe in aqueous solution studied by hyperpolarized Xe-129 NMR. *J. Inclusion Phenom. Macrocyclic Chem. 58* (1−2), 115−122.
(17) Kim, B. S., Ko, Y. H., Kim, Y., Lee, H. J., Selvapalam, N., Lee, H. C., and Kim, K. (2008) Water soluble cucurbit[6]uril derivative as a potential Xe carrier for $^{129}Xe$ NMR-based biosensors. *Chem. Commun. 24*, 2756−2758.
(18) Nikolaou, P., Coffey, A. M., Walkup, L. L., Gust, B. M., Whiting, N., Newton, H., Barcus, S., Muradyan, I., Dabaghyan, M., Moroz, G. D., Rosen, M. S., Patz, S., Barlow, M. J., Chekmenev, E. Y., and Goodson, B. M. (2013) Near-unity nuclear polarization with an open-source $^{129}Xe$ hyperpolarizer for NMR and MRI. *Proc. Natl. Acad. Sci. U. S. A. 110* (35), 14150−14155.
(19) Mugler, J. P., 3rd, and Altes, T. A. (2013) Hyperpolarized $^{129}Xe$ MRI of the human lung. *J. Magn. Reson. Imaging 37* (2), 313−331.
(20) Swanson, S. D., Rosen, M. S., Agranoff, B. W., Coulter, K. P., Welsh, R. C., and Chupp, T. E. (1997) Brain MRI with laser-polarized Xe-129. *Magn. Reson. Med. 38* (5), 695−698.
(21) Duhamel, G., Choquet, P., Grillon, E., Lamalle, L., Leviel, J. L., Ziegler, A., and Constantinesco, A. (2001) Xenon-129 MR imaging and spectroscopy of rat brain using arterial delivery of hyperpolarized xenon in a lipid emulsion. *Magn. Reson. Med. 46* (2), 208−212.
(22) Zhou, X., Mazzanti, M. L., Chen, J. J., Tzeng, Y. S., Mansour, J. K., Gereige, J. D., Venkatesh, A. K., Sun, Y., Mulkern, R. V., and Albert, M. S. (2008) Reinvestigating hyperpolarized relaxation time in the rat brain Xe-129 longitudinal with noise considerations. *NMR Biomed. 21* (3), 217−225.
(23) Zhou, X., Sun, Y. P., Mazzanti, M., Henninger, N., Mansour, J., Fisher, M., and Albert, M. (2011) MRI of stroke using hyperpolarized Xe-129. *NMR Biomed. 24* (2), 170−175.
(24) Mazzanti, M. L., Walvick, R. P., Zhou, X., Sun, Y. P., Shah, N., Mansour, J., Gereige, J., and Albert, M. S. (2011) Distribution of hyperpolarized xenon in the brain following sensory stimulation: preliminary MRI findings. *PLoS One 6* (7).
(25) Hill, P. A., Wei, Q., Eckenhoff, R. G., and Dmochowski, I. J. (2007) Thermodynamics of xenon binding to cryptophane in water and human plasma. *J. Am. Chem. Soc. 129* (37), 11662−11662.
(26) Jacobson, D. R., Khan, N. S., Colle, R., Fitzgerald, R., Laureano-Perez, L., Bai, Y., and Dmochowski, I. J. (2011) Measurement of radon and xenon binding to a cryptophane molecular host. *Proc. Natl. Acad. Sci. U. S. A. 108* (27), 10969−10973.
(27) Fairchild, R. M., Joseph, A. I., Holman, K. T., Fogarty, H. A., Brotin, T., Dutasta, J. P., Boutin, C., Huber, G., and Berthault, P. (2010) A water-soluble Xe@cryptophane-111 complex exhibits very high thermodynamic stability and a peculiar Xe-129 NMR chemical shift. *J. Am. Chem. Soc. 132* (44), 15505−15507.
(28) Fogarty, H. A., Berthault, P., Brotin, T., Huber, G., Desvaux, H., and Dutasta, J. P. (2007) A cryptophane core optimized for xenon encapsulation. *J. Am. Chem. Soc. 129* (34), 10332−10333.
(29) Hill, P. A., Wei, Q., Troxler, T., and Dmochowski, I. J. (2009) Substituent effects on xenon binding affinity and solution behavior of water-soluble cryptophanes. *J. Am. Chem. Soc. 131* (8), 3069−3077.
(30) Spence, M. M., Rubin, S. M., Dimitrov, I. E., Ruiz, E. J., Wemmer, D. E., Pines, A., Yao, S. Q., Tian, F., and Schultz, P. G. (2001) Functionalized xenon as a biosensor. *Proc. Natl. Acad. Sci. U. S. A. 98* (19), 10654−10657.
(31) Lowery, T. J., Garcia, S., Chavez, L., Ruiz, E. J., Wu, T., Brotin, T., Dutasta, J. P., King, D. S., Schultz, P. G., Pines, A., and Wemmer, D. E. (2006) Optimization of xenon biosensors for detection of protein interactions. *ChemBioChem 7* (1), 65−73.
(32) Ruiz, E. J., Sears, D. N., Pines, A., and Jameson, C. J. (2006) Diastereomeric Xe chemical shifts in tethered cryptophane cages. *J. Am. Chem. Soc. 128* (51), 16980−16988.
(33) Hilty, C., Lowery, T. J., Wemmer, D. E., and Pines, A. (2006) Spectrally resolved magnetic resonance imaging of a xenon biosensor. *Angew. Chem., Int. Ed. 45*, 70−73.
(34) Rose, H. M., Witte, C., Rossella, F., Klippel, S., Freund, C., and Schröder, L. (2014) Development of an antibody-based, modular biosensor for Xe-129 NMR molecular imaging of cells at nanomolar concentrations. *Proc. Natl. Acad. Sci. U. S. A. 111* (32), 11697−11702.
(35) Wei, Q., Seward, G. K., Hill, P. A., Patton, B., Dimitrov, I. E., Kuzma, N. N., and Dmochowski, I. J. (2006) Designing $^{129}Xe$ NMR biosensors for matrix metalloproteinase detection. *J. Am. Chem. Soc. 128* (40), 13274−13283.
(36) Chambers, J. M., Hill, P. A., Aaron, J. A., Han, Z., Christianson, D. W., Kuzma, N. N., and Dmochowski, I. J. (2009) Cryptophane xenon-129 nuclear magnetic resonance biosensors targeting human carbonic anhydrase. *J. Am. Chem. Soc. 131* (2), 563−569.
(37) Schlundt A, K. W., Beyermann, M., Sticht, J., Guenther, S., Höpner, S., Falk, K., Roetzschke, O., Mitschang, L., and Freund, C. (2009) A xenon-129 biosensor for monitoring MHC-peptide interactions. *Angew. Chem., Int. Ed. 48*, 4142−4145.
(38) Seward, G. K., Wei, Q., and Dmochowski, I. J. (2008) Peptide-mediated cellular uptake of cryptophane. *Bioconjugate Chem. 19* (11), 2129−2135.
(39) Seward, G. K., Bai, Y., Khan, N. S., and Dmochowski, I. (2011) Cell-compatible, integrin-targeted cryptophane-$^{129}Xe$ NMR biosensors. *Chem. Sci. 2*, 1103−1110.
(40) Palaniappan, K. K., Ramirez, R. M., Bajaj, V. S., Wemmer, D. E., Pines, A., and Francis, M. B. (2013) Molecular imaging of cancer cells using a bacteriophage-based $^{129}Xe$ NMR biosensor. *Angew. Chem., Int. Ed. 52* (18), 4849−4853.
(41) Klippel, S., Dopfert, J., Jayapaul, J., Kunth, M., Rossella, F., Schnurr, M., Witte, C., Freund, C., and Schröder, L. (2014) Cell tracking with caged xenon: using cryptophanes as MRI reporters upon cellular internalization. *Angew. Chem., Int. Ed. 53* (2), 493−496.
(42) Boutin, C., Stopin, A., Lenda, F., Brotin, T., Dutasta, J. P., Jamin, N., Sanson, A., Boulard, Y., Leteurtre, F., Huber, G., Bogaert-Buchmann, A., Tassali, N., Desvaux, H., Carriere, M., and Berthault, P.

(2011) Cell uptake of a biosensor detected by hyperpolarized Xe-129 NMR: The transferrin case. *Biorg. Med. Chem. 19* (13), 4135−4143.
(43) Matherly, L. H., and Goldman, D. I. (2003) Membrane transport of folates. *Vitam. Horm. 66*, 403−456.
(44) Qiu, A., Jansen, M., Sakaris, A., Min, S. H., Chattopadhyay, S., Tsai, E., Sandoval, C., Zhao, R., Akabas, M. H., and Goldman, I. D. (2006) Identification of an intestinal folate transporter and the molecular basis for hereditary folate malabsorption. *Cell 127* (5), 917−928.
(45) Salazar, M. D., and Ratnam, M. (2007) The folate receptor: what does it promise in tissue-targeted therapeutics? *Cancer Metastasis Rev. 26*, 141−152.
(46) Elnakat, H., and Ratnam, M. (2004) Distribution, functionality and gene regulation of folate receptor isoforms: implications in targeted therapy. *Adv. Drug Delivery Rev. 56*, 1067−1084.
(47) Sudimack, J., and Lee, R. J. (2000) Targeted drug delivery via the folate receptor. *Adv. Drug Delivery Rev. 41* (2), 147−162.
(48) Hilgenbrink, A. R., and Low, P. S. (2005) Folate receptor-mediated drug targeting: from therapeutics to diagnostics. *J. Pharm. Sci. 94* (10), 2135−2146.
(49) Toffoli, G., Cernigoi, C., Russo, A., Gallo, A., Bagnoli, M., and Boiocchi, M. (1997) Overexpression of folate binding protein in ovarian cancers. *Int. J. Cancer 74* (2), 193−198.
(50) Wu, M., Gunning, W., and Ratnam, M. (1999) Expression of folate receptor type alpha in relation to cell type, malignancy, and differentiation in ovary, uterus, and cervix. *Cancer Epidemiol. Biomarkers Prev. 8* (9), 775−782.
(51) Wang, S., and Low, P. S. (1998) Folate-mediated targeting of antineoplastic drugs, imaging agents, and nucleic acids to cancer cells. *J. Controlled Release 53* (1−3), 39−48.
(52) Bartik, K., Luhmer, M., Dutasta, J. P., Collet, A., and Reisse, J. (1998) Xe-129 and H-1 NMR study of the reversible trapping of xenon by cryptophane-A in organic solution. *J. Am. Chem. Soc. 120* (4), 784−791.
(53) Wender, P. A., Mitchell, D. J., Pattabiraman, K., Pelkey, E. T., Steinman, L., and Rothbard, J. B. (2000) The design, synthesis, and evaluation of molecules that enable or enhance cellular uptake: peptoid molecular transporters. *Proc. Natl. Acad. Sci. U. S. A. 97* (24), 13003−13008.
(54) Punna, S., Kuzelka, J., Wang, Q., and Finn, M. G. (2005) Head-to-tail peptide cyclodimerization by copper-catalyzed azide-alkyne cycloaddition. *Angew. Chem., Int. Ed. Engl. 44*, 2215−2220.
(55) Rostovtsev, V. V., Green, L. G., Fokin, V. V., and Sharpless, K. B. (2002) A stepwise Huisgen cycloaddition process: Copper(I)-catalyzed regioselective "ligation" of azides and terminal alkynes. *Angew. Chem., Int. Ed. Engl. 41* (14), 2596−2599.
(56) Tornøe, C. W., Christensen, C., and Meldal, M. (2002) Peptidotriazoles on solid-phase: [1,2,3]-Triazoles by regiospecific copper(I)-catalyzed 1,3-dipolar cycloadditions of terminal alkynes to azides. *J. Org. Chem. 67* (9), 3057−3064.
(57) Nomura, M., Shuto, S., and Matsuda, A. (2000) Development of an efficient intermediate, alpha-[2-(trimethylsilyl)ethoxy]-2-N- [2-(trimethylsilyl)ethoxycarbonyl]folic acid, for the synthesis of folate (gamma)-conjugates, and its application to the synthesis of folate-nucleoside conjugates. *J. Org. Chem. 65* (16), 5016−5021.
(58) Atherton, E., and Sheppard, R. C. (1989) *Solid-Phase Peptide Synthesis*, pp 1−203, Oxford.
(59) Leffler, J. E., and Temple, R. D. (1967) Staudinger reaction between triarylphosphines and azides. Mechanism. *J. Am. Chem. Soc. 89*, 5235−5246.
(60) Taratula, O., Kim, M. P., Bai, Y. B., Philbin, J. P., Riggle, B. A., Haase, D. N., and Dmochowski, I. J. (2012) Synthesis of enantiopure, trisubstituted cryptophane-A derivatives. *Org. Lett. 14* (14), 3580−3583.
(61) Leamon, C. P., and Low, P. S. (2001) Folate-mediated targeting: from diagnostics to drug and gene delivery. *Drug Discovery Today 6* (1), 44−51.
(62) Moon, W. K., Lin, Y. H., O'Loughlin, T., Tang, Y., Kim, D. E., Weissleder, R., and Tung, C. H. (2003) Enhanced tumor detection using a folate receptor-targeted near-infrared fluorochrome conjugate. *Bioconjugate Chem. 14* (3), 539−545.
(63) Kim, I. B., Shin, H., Garcia, A. J., and Bunz, U. H. (2007) Use of a folate-PPE conjugate to image cancer cells in vitro. *Bioconjugate Chem. 18* (3), 815−820.
(64) Leamon, C. P., and Low, P. S. (1991) Delivery of macromolecules into living cells: a method that exploits folate receptor endocytosis. *Proc. Natl. Acad. Sci. U. S. A. 88* (13), 5572−5576.
(65) Collet, A. (1987) Cyclotriveratrylenes and cryptophanes. *Tetrahedron 43* (24), 5725−5759.
(66) Kaarsholm, N. C., Kolstrup, A. M., Danielsen, S. E., Holm, J., and Hansen, S. I. (1993) Ligand-induced conformation change in folate-binding protein. *Biochem. J. 292* (Pt3), 921−925.
(67) Shapiro, M. G., Ramirez, R. M., Sperling, L. J., Sun, G., Sun, J., Pines, A., Schaffer, D. V., and Bajaj, V. S. (2014) Genetically encoded reporters for hyperpolarized xenon magnetic resonance imaging. *Nat. Chem. 6* (7), 630−635.
(68) Taratula, O., Hill, P. A., Bai, Y., Khan, N. S., and Dmochowski, I. J. (2011) Shorter synthesis of trifunctionalized cryptophane-A derivatives. *Org. Lett. 13* (6), 1414−1417.
(69) Brotin, T., Roy, V., and Dutasta, J. P. (2005) Improved synthesis of functional CTVs and cryptophanes using $Sc(OTf)_3$ as catalyst. *J. Org. Chem. 70* (16), 6187−6195.